Green synthesis of Ag and Au NPs decorated rGO nanocomposite for high impedimetric electrochemical sensor as well as enhanced antimicrobial performance against foodborne pathogens

Chandran Krishnaraj [a,b,1], Sivaprakasam Radhakrishnan [c,1], Misgana Mengistu Asmare [a,b], Shahid Wahab [a,b], Byoung-Suhk Kim [c,d], Soon-Il Yun [a,b,*]

[a] *Department of Food Science and Technology, College of Agriculture and Life Sciences, Jeonbuk National University, 567 Baekje-daero, Deokjin-gu, Jeonju-si, Jeollabuk-do 54896, Republic of Korea*
[b] *Department of Agricultural Convergence Technology, College of Agriculture and Life Science, Jeonbuk National University, 567 Baekje-daero, Deokjin-gu, Jeonju-si, Jeollabuk-do 54896, Republic of Korea*
[c] *Department of Organic Materials & Fiber Engineering, Jeonbuk National University, 567 Baekje-daero, Deokjin-gu, Jeonju-si, Jeollabuk-do 54896, Republic of Korea*
[d] *Department of Carbon Composites Convergence Materials Engineering, Jeonbuk National University, 567 Baekje-daero, Deokjin-gu, Jeonju-si, Jeollabuk-do 54896, Republic of Korea*

ARTICLE INFO

ABSTRACT

In the present study, *Allium cepa* L. leaves extract mediated silver nanoparticles (AgNPs) and gold nanoparticles (AuNPs) decorated reduced graphene oxide (Ag/Au/rGO NC's) were synthesized and demonstrated their biological and electrochemical sensing applications. Interestingly, the synthesis of AgNPs and AuNPs was achieved rapidly within 1 h and 4 h, respectively. Whereas the production of both reduced graphene oxide (rGO) and Ag/Au/rGO NC's was achieved at 96 h. The achieved results from the UV–Vis spectrum of 432 nm for AgNPs and 550 nm of AuNPs and the shifting of the characteristic GO absorption band of 230 nm into 270 nm as well as an absence of 305 nm confirmed the rGO synthesis. In addition, HR-XRD analyses confirmed the JCPDS file No. 04–0783 and 01–1174 pertaining to Ag and Au NPs. Further, the Raman spectroscopy, FT-IR and EDS analyses confirmed the evidence of nanomaterials biosynthesis. A polydisperse, spherical shaped average size AgNPs of 1 to 30 nm, spherical and triangular shaped AuNPs with an average size of 1 to 120 nm, and silk like appearance of a thin layered graphene sheet in rGO were observed through TEM. Also, the recorded results evident the uniform decoration of Ag and Au NPs into the rGO sheet. The electrochemical properties of as-synthesized materials were studied by electrochemical impedance spectroscopic (EIS) and cyclic voltammetry (CV) techniques. Interestingly, the Ag/Au/rGO NC's modified electrode exhibited higher electrical conductivity and good electrocatalytic properties towards the electrooxidation of nitrite in a neutral medium than other nanomaterials. Eventually, Ag/Au/rGO NC's confirmed the enhanced antibacterial against Gram-negative bacteria and dose dependent antifungal inhibitory activities against foodborne fungal pathogens of *Fusarium graminearum*, *Alternaria alternata,* and phytopathogenic fungus of *Curvularia lunata* and *Sclerotinia sclerotiorum* at the maximum tested conc. of 2 mg/mL, compared to other nanomaterials. From the result of zebrafish embryotoxicity (ZET), the highest toxicity was observed for AgNPs at 0.19 μg/mL. But in the case of Ag/Au/rGO NC's the reduced toxicity was observed. Hence, the achieved results concluded the Ag/Au/rGO NC's could be suitable for development of both as biomaterials for biomedical and effective sensors for environmental applications.

1. Introduction

Graphene has the highest hardness and durability of any two-dimensional (2D) atomic material, possessing an exceptional amount of electronic, mechanical, and chemical properties (Geim & Novoselov, 2007; Maddinedi, et al., 2015). It is an incredibly thin material that can be transformed into many kinds of surfaces. This is owing to the superior thermal power and electrical conductivity of graphene in conjunction with its excellent elasticity and flexibility, which make the material a great candidate for many device applications. The material has been regarded as promising for an extensive range of applications in terms of biochemical sensors (Lu, et al., 2009), nanoelectronics devices (Xuan, et al., 2008), field effect transistors (Stine, et al., 2010), transparent conductive films (Zheng, et al., 2014), electro responsive actuators (Zhang, et al., 2021b), flexible optoelectronic, photonic and electronic devices (Wu, et al., 2023), energy and data storage systems (Tian, et al., 2021) and much more. By reductive processes that turn graphene oxide (GO) into reduced graphene oxide (rGO). As GO is reduced, certain groups like carboxyl groups (–COOH), hydroxyl groups (–OH), and epoxy groups (-O-) are removed from its surface by a reducing agent, resulting in rGO, which exhibits many of the same properties as graphene (Liu, et al., 2019). However, during the reduction processes, the re-staking of graphene sheets resulted in the loss of active surface area, which, in turn, disrupted its possible applications. In addition to decreasing the stacking interactions between metallic nanoparticles (MNPs) on graphene sheets, it is possible to minimize the tendency for aggregation by decorating the sheets with MNPs (Moghayedi, et al., 2017).

In the past decade, nanotechnology emerged as a dynamic research area with a developing scientific interest around the globe. The use of MNPs such as AgNPs and AuNPs dates to the earliest centuries of human civilization due to their expected non-toxic antimicrobial and biomedical properties, respectively. Further, the recent advancements in the field of biomedical, the use of MNPs is versatile in a variety of applications (Ge, et al., 2014), such as antimicrobial gel formulation (Jain, et al., 2009), NPs aided wound healing dressings (Rigo, et al., 2013), orthopedic operations (Brennan, et al., 2015), medical catheters (Lackner, et al., 2008), blood-contacting implants (De Mel et al., 2012), endodontic filling materials (Bahador, et al., 2015), dental instruments (Murphy, et al., 2015) and coating of contact lenses (Willcox, et al., 2010). It is also widely known to exhibit strong antibacterial, antifungal, and antiviral activities aided by its small size and larger surface area (Franci, et al., 2015). Apart from biomedical applications, nanocomposite materials widely contributed to the degradation of methylene blue (Ibrahim et al., 2021), rhodamine b (Alshorifi et al., 2022), and photodegradation and hydrogen evolution (Mannaa et al., 2021) studies.

Recently, plant extract-based synthesis of AgNPs (Shah, et al., 2021), AuNPs (Singh & Mijakovic, 2022), rGO (Maddinedi, et al., 2015), rGO/AgNPs (Krishnaraj, et al., 2022a), rGO/AuNPs (El-Maghrabi et al., 2021) and rGO/Ag/Au NCs (Hazarika, et al., 2017) were successfully produced and applied into a wide area of applications. These successful fabrications were feasible due to the presence of phytoconstituents especially, quercetin, saponin, phenolic group, polyphenol, aromatic amine, alkaloid, flavone, terpenoid, catechin gallate, ascorbic acid and proteins (Rajan et al., 2015). Plant-based AgNPs typically possess distinctive chemical, physical, and biological properties. Reports have indicated that they exhibit potent and wide-ranging bactericidal effects against both Gram-positive and Gram-negative bacterial strains (Iravani, et al., 2014). Plant-based AgNPs-impregnated dressings with minimal or no cytotoxicity are considered exceptionally safe for patients with severe wounds (Velázquez-Velázquez, et al., 2015). A study reported that the silver (Ag) within AgNPs is potent in generating reactive oxygen species (ROS) within cells, leading to elevated calcium levels, membrane disruption, exposure of phosphatidylserine on the outer membrane, DNA degradation, and activation of caspase-like proteins (Lee, et al.,

2014). A recent study also suggested that the synthesis of AgNPs from plant extracts effectively inhibits the growth of several pathogenic bacteria and fungi (Patra & Baek, 2016). Our findings align with those of Buszewski et al. (2018), who observed a similar inhibitory effect on the growth of *P. aeruginosa* and *S. aureus* when treated with bioactive AgNPs.

Similarly, plant-based gold nanoparticles (AuNPs) exhibit significant antimicrobial potential. Their unique physicochemical properties, such as high surface activity, large-scale specific surface area, and excellent biocompatibility, have garnered the attention of biomedical researchers in recent years (Cai, et al., 2017). Many studies have recently reported the antibacterial, antiviral, and antifungal activities of plant-based AuNPs. For instance, Boomi, et al. (2020) reported the remarkable inhibition zones against *S. epidermidis* and *E. coli* when treated with AuNPs engineered from the aqueous extract of *Acalypha indica*. This study suggests that plant-based AuNPs are effective against both G^+ and G^- bacterial strains. Similarly, Khatua, et al. (2020) reported that AuNPs were effective fungicidal when they tested the antifungal activity of *Pongamia pinnata* based AuNPs against Oomycetes suggesting that plant-based AuNPs possess tremendous antimicrobial potential. Additionally, the green synthesis of Ag/Au/rGO nanocomposites involves the incorporation of AgNPs, AuNPs, and rGO, utilizing plant extracts as both reductants and stabilizers (Hazarika, et al., 2017). These nanocomposites have demonstrated enhanced properties, including improved stability, biocompatibility, and antimicrobial efficacy when compared to individual nanoparticles. They have also found utility in a variety of applications, including biosensors, catalysts, and antimicrobial agents.

Several recent studies have reported on the embryotoxicity of plant-based MNPs and their mechanisms in relation to zebrafish. In our previous research, the highest embryotoxicity was reported using AgNPs and SeNPs. Intriguingly, reduced toxicity was observed for Cs NPs, followed by Cs/Se NCs and Cs/Ag NCs, attributed to the presence of the Cs matrix (Krishnaraj, et al., 2022b). In another study, AgNPs, rGO, and rGO/AgNPs were synthesized using *Angelica keiskei* leaves extract and performed its embryotoxicity against zebrafish in which the toxic effect was significantly reduced in the presence of rGO matrix of rGO/AgNPs composite compared to AgNPs (Krishnaraj, et al., 2022a). Apart from AgNPs decoration on the rGO matrix a recent study was also focused on a combination of different concentrations of $Fe_3O_4@Au/rGO$ NSs against KB oral squamous carcinoma cell line and photothermal therapy (Ardakani, et al., 2020; Ardakani, et al., 2021) respectively, $CoFe_2O_4@rGO$ for magneto-antibacterial against Gram-negative bacteria (Meidanchi, 2020). All those researches indicate the wide acceptance of MNPs on the rGO matrix which exhibits tremendous applications. With this background knowledge, the present study aimed to reduce the toxic effects of Ag/Au/rGO NCs synthesized using *Allium cepa L.* (Onion) leaves extract. Additionally, the detection of nitrite compounds using the as-synthesized nanomaterials was proposed. It is well-known that the nitrite ion is one of the important compounds in the pharmaceutical and chemical industries (Radhakrishnan, et al., 2014). Further, the nitrite ion is also broadly used as a preservative in various processed food items (Nasraoui, et al., 2021). Hence, the screening of nitrite ions by a simple method is highly useful for various industries. The plant *Allium cepa* L. used in the present study belongs to the "*Amaryllidaceae*" family. *Allium cepa* L. is rich in phytochemicals such as phenolic compounds like flavonoids, quercetin, ferulic acid, and glycosides (Mnayer, et al., 2014). *A. cepa* L. has bioreduction capabilities and hence acts as a reducer for AgNPs synthesis (Lekshmi, et al., 2012) and AuNPs with microbicidal effects (Parida, et al., 2011).

2. Materials and methods

2.1. Materials

The *Allium cepa* L. leaves were procured from a local supermarket

located in Jeonju City, Jeollabuk-do. Graphene oxide (2 mg/mL), silver nitrate, gold (III) chloride trihydrate, MTT, DCFH-DA, nafion (5 wt%), and sodium nitrite were received from Sigma Aldrich and suitable microbial media were received from Difco. The ATCC strain number 14,579 of *B. cereus* and 14,028 of *S. typhimurium* were received from the American Type Culture Collection. The KCTC 1927 strain of *S. aureus* was received from the Korean Collection of Type Cultures and the KCCM 11234 strain of *E. coli* was received from the Korean Culture Centre of Microorganisms. The foodborne (*Fusarium graminearum, Alternaria alternata)* and phytopathogenic (*Curvularia lunata, Sclerotinia sclerotiorum)* fungal strains were received from the Korean Agriculture Culture Collection (KACC) center, S. Korea.

2.2. Extract preparation

The healthy and cleaned (*Allium cepa* L.) leaves (25 g) were cut into small pieces and boiled in 250 mL of D.H$_2$O using the oven for 6 min, then filtered through Whatman grade 5 qualitative filter paper and kept at room temperature to cool for nanomaterials synthesis.

2.2.1. AgNPs synthesis

The 24 mL of *A. cepa* extract with 176 mL of D.H$_2$O and the addition of 1 mM AgNO$_3$ resulted in AgNPs formation. To reduce the photoactivation effect, it was covered with aluminum foil and kept in a shaker at 110 rpm and the sample was drawn periodically to study under UV–Vis spec. (Hewlett Packard (HP 8453).

2.2.2. AuNPs synthesis

For AuNPs synthesis, 20 mL of prepared extract was mixed with 80 mL of sterile D·H$_2$O, addition of 1 mM HAuCl$_4$.3H$_2$O, and kept under dark for 4 h. Then the reactant was examined using UV–Vis spec. (Hewlett Packard (HP 8453).

2.2.3. rGO synthesis

Similarly, for rGO synthesis, 50 mL of the extract was mixed with 2 mL of GO and kept under shaking conditions at 120 rpm for 4 days. Frequent sampling was done and investigated using UV–Vis spec. to confirm the initial nanomaterials formation (Hewlett Packard (HP 8453).

2.2.4. Ag/Au/rGO NC's

Eventually, for nanocomposite preparation, 50 mL of *A. cepa* extract with 2 mL of GO and the addition of 1 mM HAuCl$_4$.3H$_2$O and 1 mM AgNO$_3$ resulted in the formation of nanocomposite by incubating the setup under dark in a shaker at 120 rpm for 4 days. Frequent sampling was done to check the initial nanomaterials formation through UV–Vis spec. (Hewlett Packard (HP 8453).

2.3. Nanomaterials characterization

Based on preliminary confirmation from UV–Vis spec, the reactants were centrifuged using an ultrahigh-speed centrifuge at 14,000 rpm for 20 min. Subsequently, the collected pellets underwent multiple purification steps using D·H$_2$O and were then stored in 1 mL of DI water. TEM images were captured by placing a minimal amount (25 µL) of purified AgNPs, AuNPs, rGO, and Ag/Au/rGO NCs onto a suitable grid. Additionally, a known quantity of the excess reaction material was stored at −80 °C, freeze-dried using a floor freeze drier from IlShin Lab. Co. Ltd. (FD5508), and the dried powders were examined using HR-XRD (Bruker D8 advance), FT-IR (Perkin Elmer), Raman spectroscopy (Raman Touch) and EDS (Carl Zeiss SUPRA40VP).

2.4. Nanomaterials modified electrode

The glassy carbon electrode (GCE) was initially cleaned by alumina suspension and then sonicated in water and ethanol for 3 min to remove impurities. A 10 µL of as-prepared nanomaterials (rGO, AgNPs, AuNPs, Ag/Au/rGO NC's) were (2 mg in a mixture of 50 µL Nafion and 450 µL of water) drop-cast over the pre-cleaned glassy carbon electrode and kept it to dry at room temperature.

2.4.1. Nitrite stock solution and phosphate buffer preparation procedure

The sodium nitrite salt was used for the preparation of nitrite stock (0.2 M) solution in phosphate buffer solution. The 0.1 M of phosphate buffer solution was prepared using sodium phosphate monobasic (NaH$_2$PO$_4$) and sodium phosphate dibasic (Na$_2$HPO$_4$) salts. The pH of the phosphate buffer solution was adjusted by phosphoric acid or 0.1 M NaOH solution. All the solution was prepared using double-distilled water.

2.4.2. Electrochemical measurement

The electrochemical measurements were performed under three-electrode configuration consisting of nanomaterials (rGO, AgNPs, AuNPs, Ag/Au/rGO NC's) modified glassy carbon electrode, Ag/AgCl (3 M KCl), and Pt wire were used as working, reference, and counter electrodes, respectively. The cyclic voltammograms were recorded in the potential window between 0.0 and 1.2 V in PBS solution containing nitrite ions. The electrochemical impedance measurements were recorded for the different modified electrodes in presence of 1 mM Fe(CN)6] 3-/4- as redox probe in 0.1 M KCl. The impedance measurement was performed in the frequency region between 0.1 Hz and 100 kHz at applied potential of 230 mV over the DC potential of 10 mV.

2.5. Mechanisms of antibacterial activity

2.5.1. Well diffusion and Minimum inhibitory concentration (MIC) assay

A common agar well diffusion assay was executed to confirm the initial antibacterial efficiency of nanomaterials as per the previous protocol with little modification (Urnukhsaikhan, et al., 2021). In brief, known concentrations (100 µL) of G$^+$ *B. cereus, S. aureus,* and G$^-$ *E. coli* and *S. typhimurium* strains were spread into suitable plates (MHA), and the wells were made using a cork borer. Then 40 µg/40 µL conc. of freeze-dried powder of *Allium cepa* extract, rGO, AgNPs, AuNPs, Ag/Au/ rGO NC's were measured and added into a suitable well and incubated the plates for 24 h at 37 °C. Further to understand the dose dependent antibacterial efficiency, a MIC of MTT was executed as per the previous protocol with little modification (Krishnaraj, et al., 2010). In brief, 100 µL of sterile media was placed into multiple well plate, 100 µg in 100 µL conc. of all the reactants were added into initial well of each row and the serial dilutions were made. Then, 100 µL of bacterial strains were added into all the well and incubated for 12 h at 37 °C. Control well also maintained for all test pathogens without dispersing the nanomaterials. Finally, known concentration of MTT (5 µL of 0.5 %) solution was supplied to all the well and the ELISA reader was used for taking the reading at (OD$_{595}$).

2.5.2. Mode of interaction and intracellular reactive oxygen species (ROS) study

To understand the antibacterial mechanistic insights of nanomaterials, the reactants were subjected to interaction against test bacteria as per previous protocol with little modification (Krishnaraj, et al., 2022b). For this, 20 mL of bacteria was spun in an ultrahigh- speed centrifugation at 6000 rpm for 10 min at 4 °C and dispersed in 2 mL of sterile D·H$_2$O. Then 1 mL of the dispersed pellet mixture was mixed with 100 µg/mL of nanomaterials and kept overnight and observed under Bio-TEM. Eventually, the ROS study was performed as the per previous protocol with little modification (Zhang, et al., 2022). Briefly, the test pathogens interacted with Ag/Au/rGO NC's for 1 h at 37 °C and washed with PBS. Then the reaction mixture was interacted at 30 min of 10 µm 2'7'-dichlorodihydrofluorescein diacetate (DCFH-DA) under dark condition and observed under CLSM at excitation wavelength of 488 nm and emission wavelength of 521 nm. Bacteria alone maintained as control.
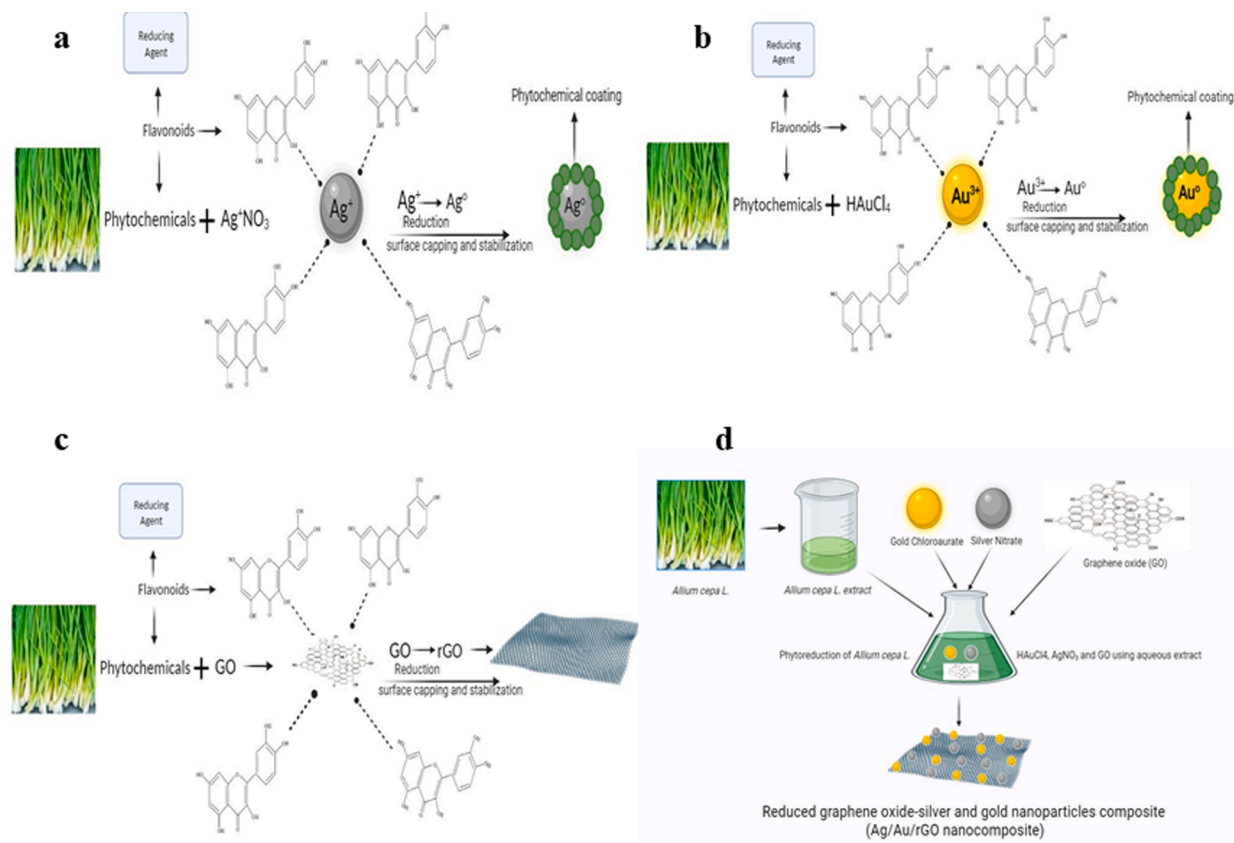
Fig. 1. Illustration shows the mechanisms involved in nanomaterials synthesis.

2.6. Antifungal activity of foodborne and phytopathogenic fungus

Antifungal activity was executed against foodborne pathogens of *Fusarium graminearum* and *Alternaria alternata* and phytopathogens of *Curvularia lunata* and *Sclerotinia sclerotiorum* using standard procedure with slight modification (Krishnaraj, et al., 2015). Briefly, 2 and 1 mg, 500 and 50 μg conc. of nanomaterials were added into Petri dishes and then PDA was poured, mixed thoroughly to get uniform dispersion of nanomaterials all over the Petridish. A fungal suspension was carefully picked up from a mother culture and spotted into Petridish in a triplicate and incubated the plates at 25 °C for 48 to 72 h. After incubation, the radial growth measurement was taken in which the radial growth of the control and the pathogens treated was measured by taking the average of the triplicates.

2.7. ZET study (Danio rerio)

The ZET assessment was done as per the previous protocol (Krishnaraj, et al., 2022b) published by our group based on Test No. 236 of FET test of OECD guidelines (Lammer, et al., 2009). In brief, 2 mL of E3 medium (Cassar, et al., 2019) containing different concentration of plant extract, rGO, AgNPs, AuNPs, Ag/Au/rGO NC's were prepared (0.09, 0.19, 0.39, 0.78, 1.56, 3.12, 6.25, 12.5, 25, 50, 100 and 200 μg/mL) using multiple well plate and then 3 hpf of healthy embryos were carefully transferred into each well and incubated at 28.5 °C in an embryo breeding chamber. The coagulation, hatching delay, edema in yolk sack, spine bent, tail bent and improper development was monitored through a stereomicroscope at different end points of 24,48, 72 and 96 hpf.

2.8. Statistical analysis

Biological analysis was carried out in triplicates and the outcome was produced by calculating the average of $\pm$ standard deviation.

3. Results and discussion

3.1. Mechanisms involved in nanomaterials synthesis

In the present study, 1 to 30 nm sizes of AgNPs and 1 to 120 nm sizes of AuNPs, silk like appearance of thin rGO sheet as well as uniform decoration of Ag and Au NPs on rGO sheet were successfully synthesized using *Allium cepa* L. leaves extract as reducing and stabilizing agents. It is believed that the synthesis mechanisms are mainly involved in the presence of any of the phenolic compounds in *Allium cepa* L. such as flavonoids, quercetin, ferulic acid, and glycosides (Fig. 1). This statement is true because previously, Khanam & Hasan (2019) had successfully reduced the graphene from GO using *Allium cepa L.* and concluded that the presence of antioxidants and vitamin c act as reducer and stabilizer. Similarly, Baran et al. (2023) and Ipek et al. (2023) synthesized AgNPs and AuNPs respectively, from *Allium cepa* L. peel extract and studied their antioxidant, antipathogenic, and anticholinesterase activities. Hence based on the background knowledge, the present study also demonstrated the successful synthesis of AgNPs, AuNPs, rGO, Ag/Au/rGO NC's from *Allium cepa* L. extract and studied their nitrite sensor, enhanced antibacterial, antifungal as well as toxicity using zebrafish embryo's.

3.2. Nanomaterials synthesis and UV–Vis spectral analysis

Twenty-four mL of the extract with 176 mL of D.H$_2$O and the addition of 1 mM AgNO$_3$ resulted in AgNPs. The primary synthesis was confirmed by a change in color formation from 1 h of incubation under dark and at 432 nm the characteristic absorption peak was observed (Supplementary Fig. S1d). Similarly, 20 mL of extract mixed with 80 mL of D.H$_2$O along with 1 mM HAuCl$_4$.3H$_2$O supported the growth of
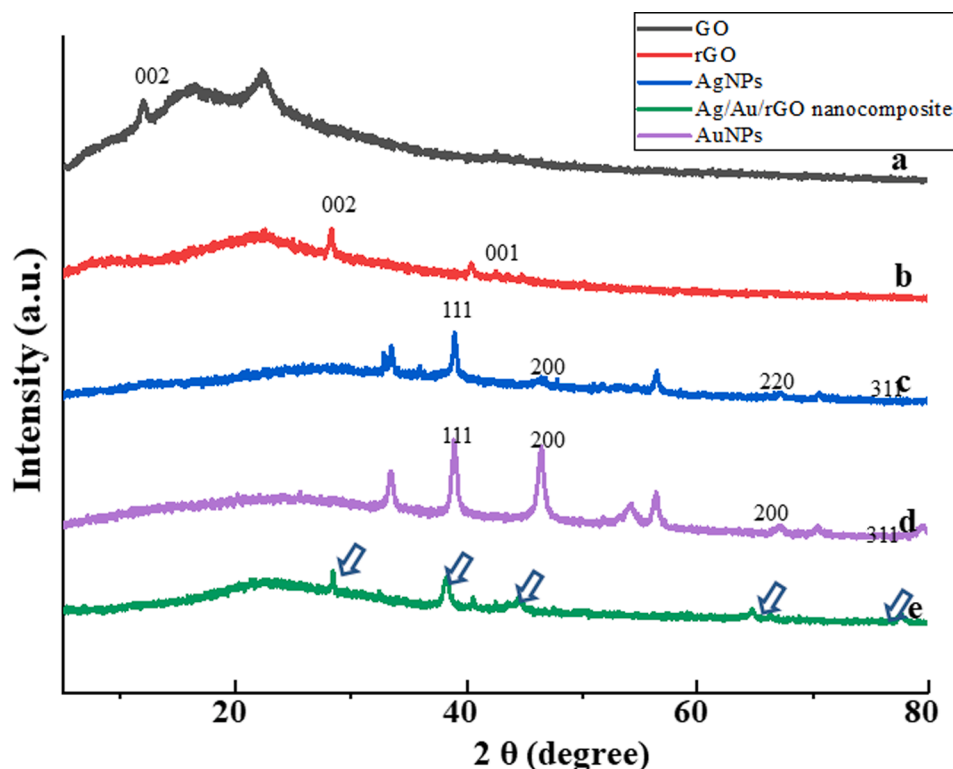
Fig. 2. HR-XRD spectra of (a) GO (b) rGO (c) AgNPs (d) AuNPs (e) Ag/Au/rGO NC's.
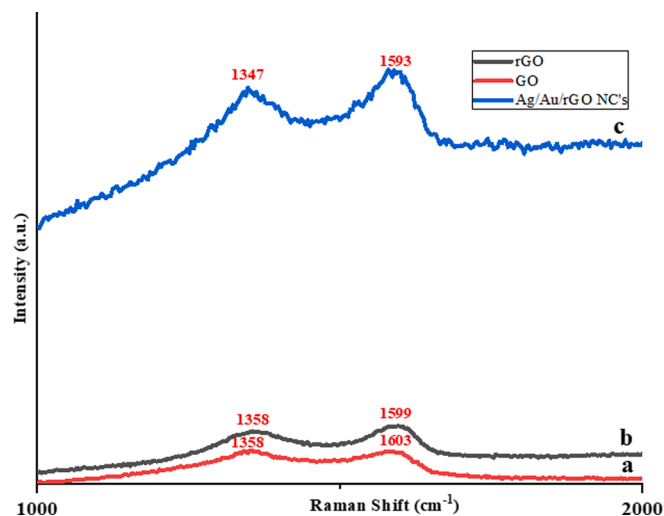
Fig. 3. Raman spectra of (a) GO (b) rGO (c) Ag/Au/rGO NC's.

AuNPs. The initial formation was confirmed by visual pale-yellow color into pinkish violet of 4 h incubation under dark and at 550 nm the characteristic absorption peak was observed (Supplementary Fig. S1e). Our achieved results agree with the recent research paper published using *Plantago lanceolata* extract for AgNPs (Shah, et al., 2021) and for AuNPs (Singh & Mijakovic, 2022). In addition, 100 mL of *Allium cepa* extract and 4 mL of GO supported the rGO formation by turning the brownish yellow into black color (Supplementary Fig. S1c) of 96 h. Whereas, no change in color was observed for commercially purchased GO (Supplementary Fig. S1b) and the characteristic absorption spectrum exhibited at 230 nm indicates the π-π* transitions of C–C bond and 305 nm denotes the n-π* electronic transition of C=O bond (Krishnaraj, et al., 2022a). Interestingly, the characteristic absorption band from 230 nm shifted to 270 nm and the absence of a peak at 305 nm was

observed in rGO sample confirming the shuffling of electrons (Li & Liu, 2010). Eventually, the 50 mL of *Allium cepa* extract and the addition of 2 mL GO along with 1 mM HAuCl$_4$.3H$_2$O and 1 mM AgNO$_3$ supported the growth of Ag/Au/rGO NC's within 96 h by continuous shaking, and the color was changed from brownish yellow into brownish black. The characteristic absorption band pertaining to GO was shifted from 230 to 260 nm and the characteristic metal nanoparticles peak confirmed the formation of Ag/Au/rGO NC's (Supplementary Fig. S1f). There was no change of color observed for plant extract alone throughout the experiment (Supplementary Fig. S1a). Similar to the present findings, *Albizia saman* leaf extract mediated synthesis of gold/silver nanobimetallics smartened rGO was performed and confirmed the respective characteristic absorption maxima through UV–Vis spec (Vellaichamy & Periakaruppan, 2016).

3.3. Nanomaterials characterization

3.3.1. HR-XRD analysis

The HR-XRD analysis was performed to characterize the crystal structure of as-synthesized nanomaterials and the data was presented in Fig. 2. The comparison of commercially purchased GO and rGO was performed in which GO (Fig. 2a) displayed a sharp peak at 2θ values of ∼ 11.2° (0 0 2) (Moon, et al., 2010). Interestingly after interaction with *Allium cepa* L. leaves extract, the existing peak disappeared and the fresh peak was formed at 2θ values of ∼ 28.1° (0 0 2) (Krishnaraj, et al., 2022a), due to the removal of oxygen moieties (Maddinedi, et al., 2015), and this indicates the bio reduction of GO into rGO (Fig. 2b). In addition, the new peak formed at ∼ 42.5° (0 0 1) which was connected to turbostratic group. Similarly, the HR-XRD pattern of AgNPs was presented in Fig. 2c, in which the diffraction peaks were observed at 2θ values of ∼ 33.2°, ∼ 35.8°, ∼ 38.8°, ∼ 44.8°, ∼ 46.4°, ∼ 47.8°, ∼ 56.6°, ∼ 64.4°, ∼ 67.1°, ∼ 70.6° and ∼ 77.3°. In this, the characteristic peaks of ∼ 38.8°, ∼ 44.8°, ∼ 64.4° and ∼ 77.3° were matched with the JCPDS file No. 04–0783 related to plane values of 1 1 1, 2 0 0, 2 2 0 and 3 1 1 cubic phases of Ag (Muddassir, et al., 2022). The possibilities of other peaks
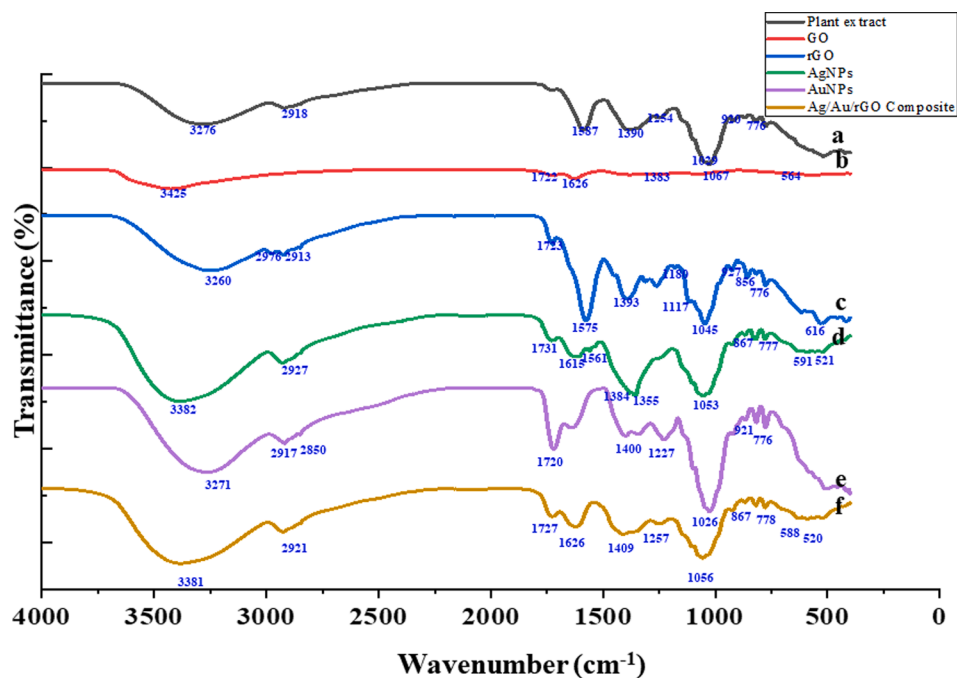
Fig. 4. FT-IR analysis of (a) Plant extract (b) GO (c) rGO (d) AgNPs (e) AuNPs (f) Ag/Au/rGO NC's.
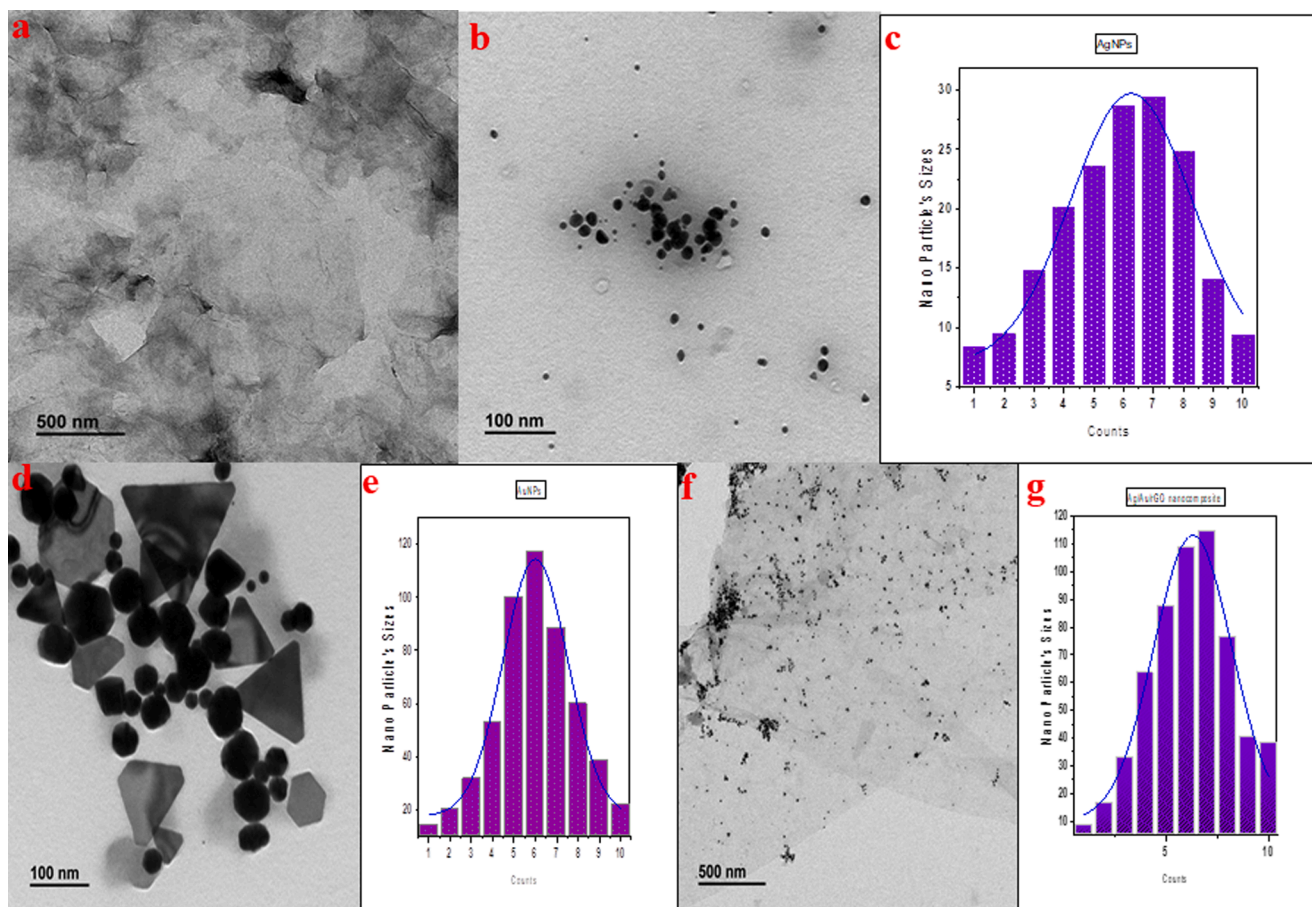
Fig. 5. TEM images of (a) rGO (b) AgNPs (d) AuNPs (f) Ag/Au/rGO NC's. Particle size distribution data of (c) AgNPs (e) AuNPs (g) Ag/Au/rGO NC's.

are due to secondary metabolite presence in *A. cepa* L. leaves extract. Similarly, the HR-XRD pattern of AuNPs was presented in Fig. 2d, in which diffraction peaks observed at $\sim 33.6°$, $\sim 38.4°$, $\sim 44.6°$, $\sim 54.2°$, $\sim 56.1°$, $\sim 64.8°$, $\sim 70.1°$ and $\sim 77.8°$. In this, the characteristic diffraction peaks were observed at $\sim 38.4°$, $\sim 44.6°$, $\sim 64.8°$ and $\sim 77.8°$ with corresponding miller indices of (111) (200) (220) and (311)

Table 1
Elemental composition of rGO, AgNPs, AuNPs and Ag/Au/rGO NC's.

Samples	C%	O%	Mg%	Na%	P%	S%	Cl%	K%	Ca%	Ag%	Au%
rGO	71.08	22.40	0.18	–	0.23	0.44	0.88	4.00	0.80	–	–
AgNPs	46.26	11.85	–	0.62	0.66	0.88	2.47	3.18	1.46	32.62	–
AuNPs	87.30	4.72	0.12	0.05	–	0.24	0.78	0.14	0.59	–	6.05
Ag/Au/rGO NC's	84.64	9.13	–	–	–	0.20	1.11	0.52	0.32	2.74	1.34
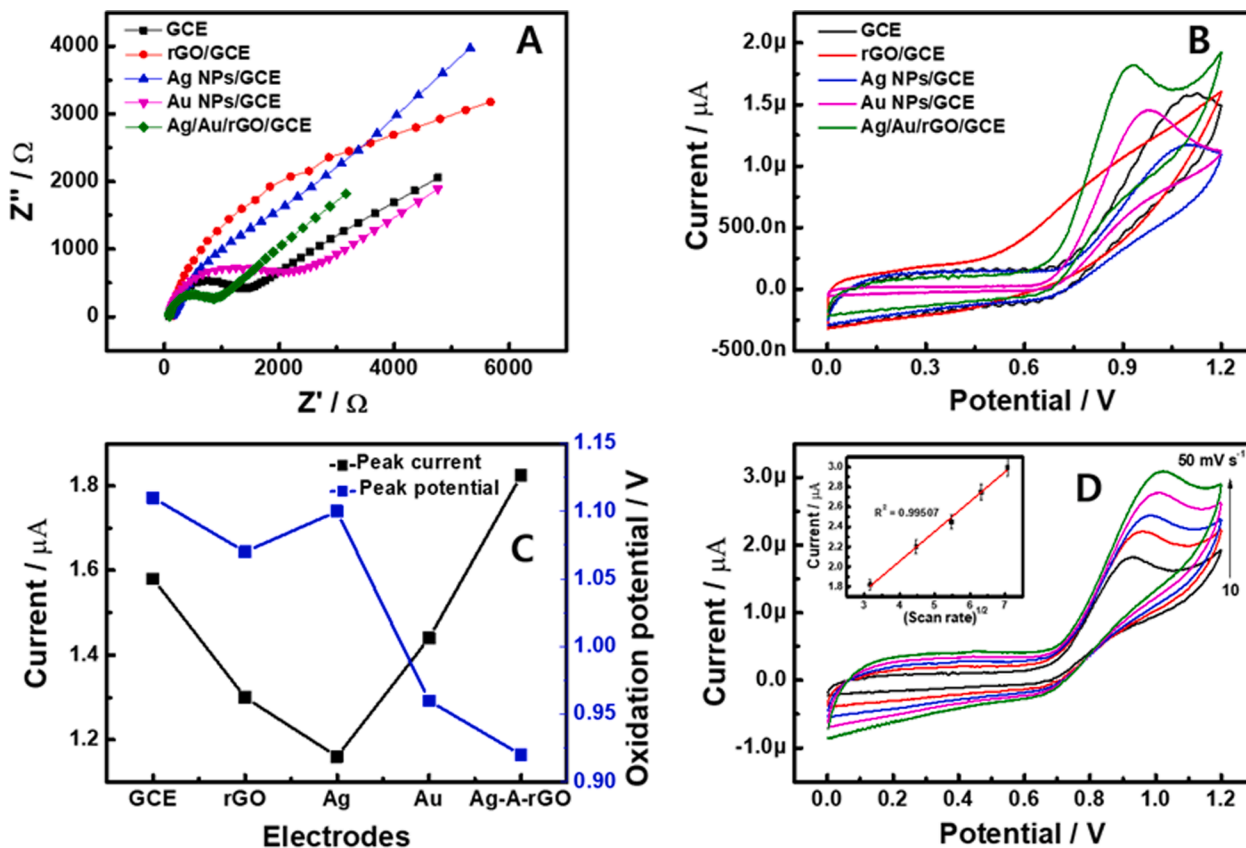
Fig. 6. (A) Electrochemical impedance spectroscopy of bare GC, rGO, Ag NPs, Au NPs and Ag/Au/rGO NC's modified electrodes in presence of 1 mM $K_4[Fe(CN)_6]^{3-/4-}$ as redox indicator in the frequency range between 100 KHz and 0.1 Hz. (B) Cyclic voltammogram (CVs) responses of different modified GC electrodes in phosphate buffer solution (PBS; pH 7.0) containing 50 µM of nitrite at scan rate of 10 mV s^{-1}. (C) Plot of nitrite oxidation peak current and oxidation peak potential against different modified electrodes. (D) CVs of Ag/Au/rGO NC's modified GC electrode in presence of 50 µM of nitrite in PBS at different scan rates from 10 –50 mV s^{-1}.

Table 2
Antibacterial activity of biologically synthesized rGO, AgNPs, AuNPs and Ag/Au/rGO NC's against pathogenic bacteria.

Bacterial pathogens	Zone of inhibition (mm in diameter)				
	Plant extract (40 µg/ 40 µL)	rGO (40 µg/ 40 µL)	AgNPs (40 µg/ 40 µL)	AuNPs (40 µg/ 40 µL)	Ag/Au/rGO NC's (40 µg/ 40 µL)
Gram-positive					
B. cereus	NZ	NZ	12 ± 1	NZ	12 ± 1
S. aureus	NZ	NZ	11 ± 1	NZ	11 ± 1
Gram-negative					
S. typhimurium	NZ	NZ	13 ± 1	NZ	13 ± 1
E. coli	NZ	NZ	13 ± 1	NZ	13 ± 1

NI: no inhibitory at maximum tested concentration (100 µg / µL). The data was presented as mean average of three independent experiments.

Table 3
Minimum Inhibitory Concentration (MIC) of biologically synthesized rGO, AgNPs, AuNPs and Ag/Au/rGO NC's against pathogenic bacteria.

Bacterial pathogens	MIC (µg / µL)				
	Plant extract	rGO	AgNPs	AuNPs	Ag/Au/rGO NC's
Gram-positive					
B. cereus	NI	NI	6.25	NI	1.56
S. aureus	NI	NI	1.56	NI	0.78
Gram-negative					
S. typhimurium	NI	NI	6.25	NI	6.25
E. coli	NI	NI	6.25	NI	6.25

NZ: no zone of inhibition. The data was presented as mean average of three independent experiments.

which are matched with the JCPDS file 01–1174 (El-Deeb, et al., 2022). The presence of other peaks was probably due to secondary metabolites involved from *A. cepa* L. leaves extract. Further, the HR-XRD pattern of

Ag/Au/rGO NC's (Fig. 2e) showed a clear diffraction peak corresponding to rGO as well as Ag and Au with 2θ values of ∼ 28°, ∼38.4, ∼40°, ∼42°, ∼44.6°, ∼64.8°, ∼77.8° which are confirmed the complete formations of composite. Arrows indicate the presence of characteristic peaks.
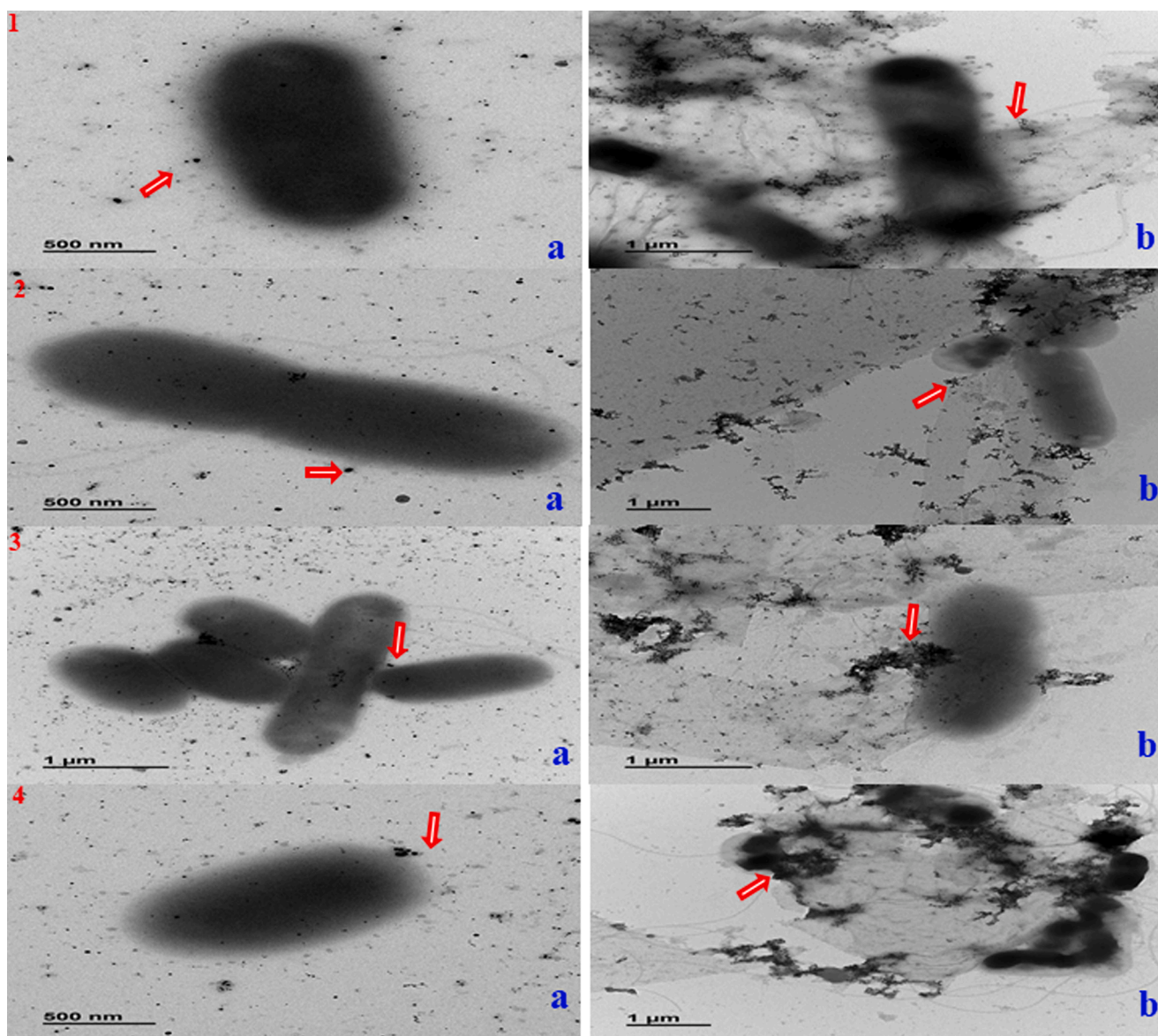
Fig. 7. Mode of interactions of (a) AgNPs (b) Ag/Au/rGO NC's against different pathogenic bacteria (1) *E. coli*; (2) *S. typhimurium*; (3) *B. cereus* (4) *S. aureus*. Arrows indicate the presence of nanomaterials.

3.3.2. Raman spec analysis

A Raman spectrum analysis was performed for GO, rGO, and Ag/Au/rGO NC's, in which the G and D band for commercially purchased GO was observed at 1603 cm^{-1} and 1358 cm^{-1}, respectively with an ID/IG band intensity of 1.01 (Fig. 3a). In case of rGO, the G and D band changed its position to 1599 cm^{-1} and 1358 cm^{-1} respectively, with an ID/IG ratio of 0.93 (Fig. 3b), and these changes were due to hexagonal structural repossession as well as structural defects in rGO of G and D band, respectively (Yaragalla, et al., 2016). The G band intensity of 1593 cm^{-1} and D band intensity of 1347 cm^{-1} was observed in Ag/Au/rGO NC's, with an ID/IG ratio of 0.96 (Fig. 3c), and this change was due to the decoration of Ag and AuNPs on the rGO surface. Our results are complemented by the previous work reported by Kumar, et al. (2016), which suggested the ID/IG ratio of the composite was higher than rGO due to the possibility of a decrease in sp^2 carbon atoms in the nanocomposite.

3.3.3. FT-IR spectral analysis

The FT-IR spectra were used to verify the nature of functional groups in the plant extract and as-derived nanomaterials. The spectra of the plant extract, and different nanomaterials derived such as GO, rGO, AgNPs, AuNPs, and Ag/Ag/rGO NC's were presented in Fig. 4. The plant extract has different organic molecules, which are highly beneficial to reducing the nanoparticles. The plant extract exhibited different peaks mainly 3276, 1587, 1390, and 1029 are linked to the –O–H, N–H, S=O, and C–H active functional groups vibrations, respectively (Zhang, et al., 2021a). The plant extract assisted synthesis of nanomaterials exhibited different peaks for all the materials including GO, rGO, AgNPs, AuNPs, and Ag/Ag/rGO NC's. Most of the peaks are perfectly matched with the plant extract peaks and peaks shift also were observed in hybrid nanomaterials. The additional peaks are due to the strong interactions between the organic functional groups and metal nanoparticles and graphene composite, which influence the characteristics peak shifts. Instance, the OH-stretching frequency of the plant extract was observed at 3276 cm^{-1}, whereas the -O–H stretching frequency was strongly shifted into 3381 cm^{-1} for the Ag/Au/rGO hybrid composite when compared to other individual nanomaterials (AgNPs, AuNPs, and rGO) prepared from plant extract due to their strong interaction of -O–H functional groups within the ternary composite material. Hence based on the findings, FT-IR spectra confirmed the successful formation of
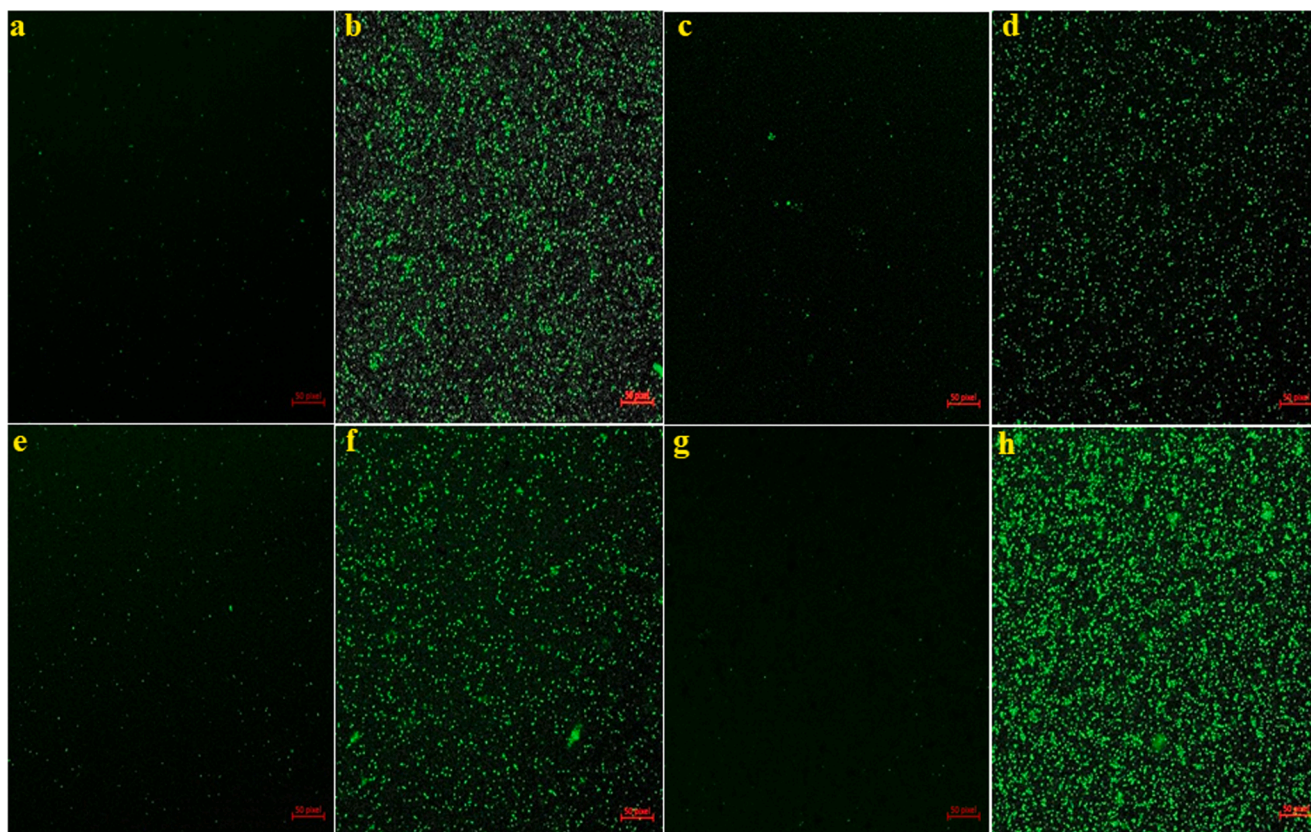
Fig. 8. Antibacterial mechanisms of Ag/Au/rGO NC's through ROS study (a) *B. cereus* control (b) *B. cereus* treated (c) *S. aureus* control (d) *S. aureus* treated (e) *E. coli* control (f) *E. coli* treated (g) *S. typhimurium* control (h) *S. typhimurium* treated.

nanomaterials through plant extract, and the functional groups are present in the as-prepared nanomaterials.

3.3.4. Electron microscopic studies

Additionally, the morphological analyses were performed through TEM (Fig. 5) in which polydispersed, spherical-shaped AgNPs of 1 to 30 nm (Fig. 5b), spherical and triangular shaped AuNPs of 1 to 120 nm (Fig. 5d) were observed. Whereas in rGO a thin layer of graphene sheets with silk like appearance was observed (Fig. 5a). Furthermore, the Ag and Au NPs were decorated almost all over the surface of rGO nanosheets, demonstrating the effective loading of NPs (Fig. 5f). In addition, particle size distribution clearly confirmed the Ag NPs (Fig. 5c) and Au NPs (Fig. 5e) were in the range of 1 to 30 nm and 1 to 120 nm respectively. Similarly, in Ag/Au/rGO NC's (Fig. 5g), a uniform decoration of Ag and Au NPs was observed in the range of 1 to 120 nm sizes.

3.3.5. EDS analysis

Table 1. confirms the overall elemental composition of rGO, AgNPs, AuNPs, and Ag/Au/rGO NC's through EDS analysis. The presence of characteristic signals such as carbon and oxygen in rGO with 77.08 % and 22.40 % respectively (Supplementary Fig. S1a), and silver with 32.62 % in AgNPs (Supplementary Fig. S1b), gold with 6.05 % in AuNPs (Supplementary Fig. S1c) and carbon, oxygen, silver and gold in nanocomposite of 84.64 %, 9.13 %, 2.74 % and 1.34 % respectively (Supplementary Fig. S1d), confirmed the maturation of composite in the reaction samples. Additional peaks like Mg, Na, P, S, Cl, K, Ca ensured the presence of other metabolites in the extract during nano formations.

3.4. Electrochemical studies of different modified electrodes

3.4.1. Electrochemical impedance spectroscopy (EIS) studies based on modified electrodes

EIS is one of the powerful electrochemical techniques for verify the electrical properties of the modified electrodes at electrode and electrolyte interface. In order to verify the electrical characteristics of the different modified electrodes were tested by EIS in 0.1 M KCl solution containing 1 mM of $[Fe(CN)_6]^{3-/4-}$ as redox probe. Fig. 6A shows the EIS spectrum of the different modified electrodes, all the EIS curves consisting of semi-circle and linear curve at higher and lower frequencies region, respectively. The diameter of the semi-circle directly linked with the insulating properties of the modified electrode. It obviously shows the diameter of the Ag/Au/rGO NC's modified electrode much lower than the other modified electrodes. The charge transfer resistance values for different modified electrodes were calculated using Randles equivalent circuit fitting with support of ZsimpWin software. The charge transfer resistance of the different modified electrodes was estimated to be 1524, 5481, 4112, 1945, and 1284 Ω for bare GCE, rGO, AgNPs, AuNPs, and Ag/Au/rGO NC's modified electrodes, respectively. It may be noted here that the charge transfer resistance for Ag/Au/rGO NC's electrode is much lower when compared to other modified electrodes and these were due to combination of different metals and rGO as well as good catalytic properties of Au and Ag NPs.

3.4.2. Cyclic voltammetry (CV) detection of nitrite using Ag/Au/rGO NC's modified electrode

The different modified electrodes were further utilized for the preliminary investigation of nitrite detection. Fig. 6B shows the CVs curves obtained for different modified electrodes including bare GC, rGO, AgNPs, AuNPs, and Ag/Au/rGO NC's modified electrodes in phosphate buffer solution (PBS) (pH 7.0) containing 50 µM nitrite at a scan rate of

Table 4
Antifungal activity of biologically synthesized rGO, AgNPs, AuNPs and Ag/Au/rGO NC's against food borne and phytopathogenic fungus.

Foodborne fungal pathogens	Radial growth in mm (Average of triplicates)				
	Control Without treatment	2 mg/mL	1 mg/mL	500 µg/mL	50 µg/mL
Fusarium graminearum					
rGO	26.0 ± 2	14.6 ± 2	16.6 ± 2	20.0 ± 2	22.0 ± 2
AgNPs		12.0 ± 2	15.6 ± 2	16.6 ± 2	19.6 ± 2
AuNPs		13.3 ± 2	16.0 ± 2	16.6 ± 2	20.3 ± 2
Ag/Au/rGO NC's		05.0 ± 2	15.3 ± 2	15.6 ± 2	16.6 ± 2
Alternaria alternata					
rGO	16.6 ± 2	11.0 ± 2	12.6 ± 2	12.6 ± 2	14.6 ± 2
AgNPs		05.0 ± 2	08.3 ± 2	09.6 ± 2	10.6 ± 2
AuNPs		05.3 ± 2	09.6 ± 2	09.6 ± 2	11.0 ± 2
Ag/Au/rGO NC's		04.0 ± 2	08.3 ± 2	09.6 ± 2	10.0 ± 2
Curvularia lunata					
rGO	14.6 ± 2	05.0 ± 2	05.6 ± 2	05.6 ± 2	08.6 ± 2
AgNPs		NRG	02.0	04.0 ± 2	05.0 ± 2
AuNPs		NRG	NRG	NRG	06.0 ± 2
Ag/Au/rGO NC's		NRG	NRG	NRG	02.0 ± 2
Sclerotinia sclerotiorum					
rGO	19.0 ± 2	03.6 ± 2	04.6 ± 2	05.0 ± 2	05.6 ± 2
AgNPs		03.6 ± 2	03.6 ± 2	04.6 ± 2	05.0 ± 2
AuNPs		03.6 ± 2	03.6 ± 2	05.0 ± 2	05.6 ± 2
Ag/Au/rGO NC's		03.6 ± 2	03.6 ± 2	04.6 ± 2	05.0 ± 2

NRG: no radial growth at tested concentrations. The data was presented as mean average of three independent experiments.

10 mV s^{-1}. All the modified electrodes were provided oxidation peak of nitrite in PBS solution. However, the oxidation peak current and peak potential were strongly affected by each modified electrode. When evaluating the oxidation peak current and peak potential values, we observed that the Ag/Au/rGO NC's modified electrode has lower oxidation peak potential and higher oxidation peak current when compared to bare GC, rGO, AgNPs, AuNPs modified electrodes. The Ag/Au/rGO NC's modified electrode delivered a higher oxidation peak current (1.824 µA) and lower oxidation peak potential (0.92 V) value when compared to other modified glassy carbon electrodes such as bare GC (1.58 µA & 1.12 V), rGO (1.3 µA & 1.1 V), AgNPs (1.17 µA & 1.07 V), AuNPs (1.44 µA & 0.96 V) (Fig. 6C). This preliminary CV investigations were clearly suggesting the present modified electrode based on Ag/Au/rGO NC's has greater potential for the electrochemical oxidation of nitrite in neutral condition. This enhanced electro-catalytic properties of Ag/Au/rGO NC's are due to the good catalytic properties from gold and silver, high electrical conductivity and surface area of the composite materials.

3.4.3. Effect of scan rate for the nitrite detection at Ag/Au/rGO NC's modified electrode

The effect of scan rate is one of the important studies to further confirm the catalytic behavior of the Ag/Au/rGO NC's modified electrode. The CV studies at various scan rates from $10 - 50$ mV s^{-1} was studied in in phosphate buffer solution (PBS) (pH 7.0) containing 50 µM of nitrite (Fig. 6D). Interestingly, the peak of oxidation current gradually increasing with increasing the potential sweeping rates. Further, a perfect linear correlation was noticed between the oxidation peak currents versus square root of scan rates (Fig. 6D), suggesting that the electro-oxidation of nitrite is diffusion-controlled process at Ag/Au/rGO NC's modified surface. This electrochemical study clearly implies that the present electrode is highly suitable for electrochemical nitrite detection. This preliminary CV studies for the electrochemical nitrite detection using Ag/Au/rGO NC's modified surface is highly useful for the electrochemical sensor for the detection of nitrite.

3.5. Nanomaterials against test bacterial pathogens – Its mechanisms

A preliminary well diffusion protocol was performed to confirm the role of nanomaterials towards bacteria and the outcome of the result was presented in Table 2. The Gram-negative bacteria of *E. coli* and *S. typhimurium* produced a good inhibition zone followed by Gram-positive bacteria of *B. cereus* and *S. aureus*, treated with AgNPs and Ag/Au/rGO NC's. The reason behind the positivity in negative bacteria was due to the outer membrane of Gram-negative bacteria is made from lipopolysaccharides (LPS) which are negatively charged. However, AgNPs have a positive charge, which can interact with the negative charge of LPS, resulting in a higher binding affinity to the outer membrane (Joshi, et al., 2020). This increased binding may lead to increased uptake of AgNPs by the bacteria, leading to higher toxicity (Gurunathan, et al., 2014). In addition, the presence of Ag & Au could have an additional effect on the antimicrobial activity of the Ag/Au/rGO NC's (Han, et al., 2020). The AuNPs combined with AgNPs have been found to have a synergistic effect, which could contribute to the increased activity against Gram-negative bacteria (Gurunathan, 2015). However, failure in producing the zone in test bacteria was observed against rGO, AuNPs, and plant extract.

Further the MIC of AgNPs and Ag/Au/rGO NC's against G⁻ test bacterial pathogens of *E. coli* and *S. typhimurium* were observed at 6.25 µg/µL conc. But in the case of G⁺ bacteria, the MIC of AgNPs against *B. cereus* and *S. aureus* was observed at 6.25 µg/µL and 1.56 µg/µL conc. Whereas, Ag/Au/rGO NC's it was observed at 1.56 and 0.78 µg/µL conc. respectively. The reason behind the effective inhibitory activity of Ag/Au/rGO NC's was due to the increased binding of AgNPs in the presence of rGO platform on the surface of a cell, based on charge attraction and the synergistic effect of AuNPs. But the absence of inhibitory activity was noted against all the test pathogens for plant extract, rGO, and AuNPs at the highest test concentration of 100 µg/µL (Table. 3). The Bio-TEM results confirmed the interaction mechanism of AgNPs and Ag/Au/rGO NC's against *E. coli* (Fig. 7(1). a-b), *S. typhimurium* (Fig. 7(2). a-b), *B. cereus* (Fig. 7(3). a-b) and *S. aureus* (Fig. 7(4). a-b). The reason behind the enhanced antibacterial activity against dose dependency was due to higher exposure of smaller sizes of nanomaterials into bacterial cells, the particles anchored several sites on the surface of negatively charged functional groups of bacterial membrane resulting in cell lysis. This statement is true, in which Tiwari et al. (2008), had done a study on the time and dose dependent antimicrobial activity of AgNPs, and concluded that enhanced antibacterial activity was observed in an increased time and dose dependent manner. In our previous work, we have also reported that based on the attraction of charge the nanomaterials bind on the surface of the cell membrane and cause cell lysis (Krishnaraj, et al., 2022a) in the presence of rGO platform and generate ROS (Yamanaka, et al., 2005), resulting in cell death. There are several studies have demonstrated that ROS plays a crucial role in the antibacterial effects of nanomaterials. One way to confirm this is by using an assay such as DCFH-DA, which can detect the presence of ROS by measuring the production of a green fluorescent substance. In the present study, Ag/Au/rGO NC's was used as a test case and found that, when compared to a control group, bacteria incubated with Ag/Au/rGO NC's emitted intense green fluorescence, indicating that these nanomaterials can facilitate ROS production (Fig. 8). High levels of ROS can lead to oxidative stress, which can ultimately result in bacterial death.
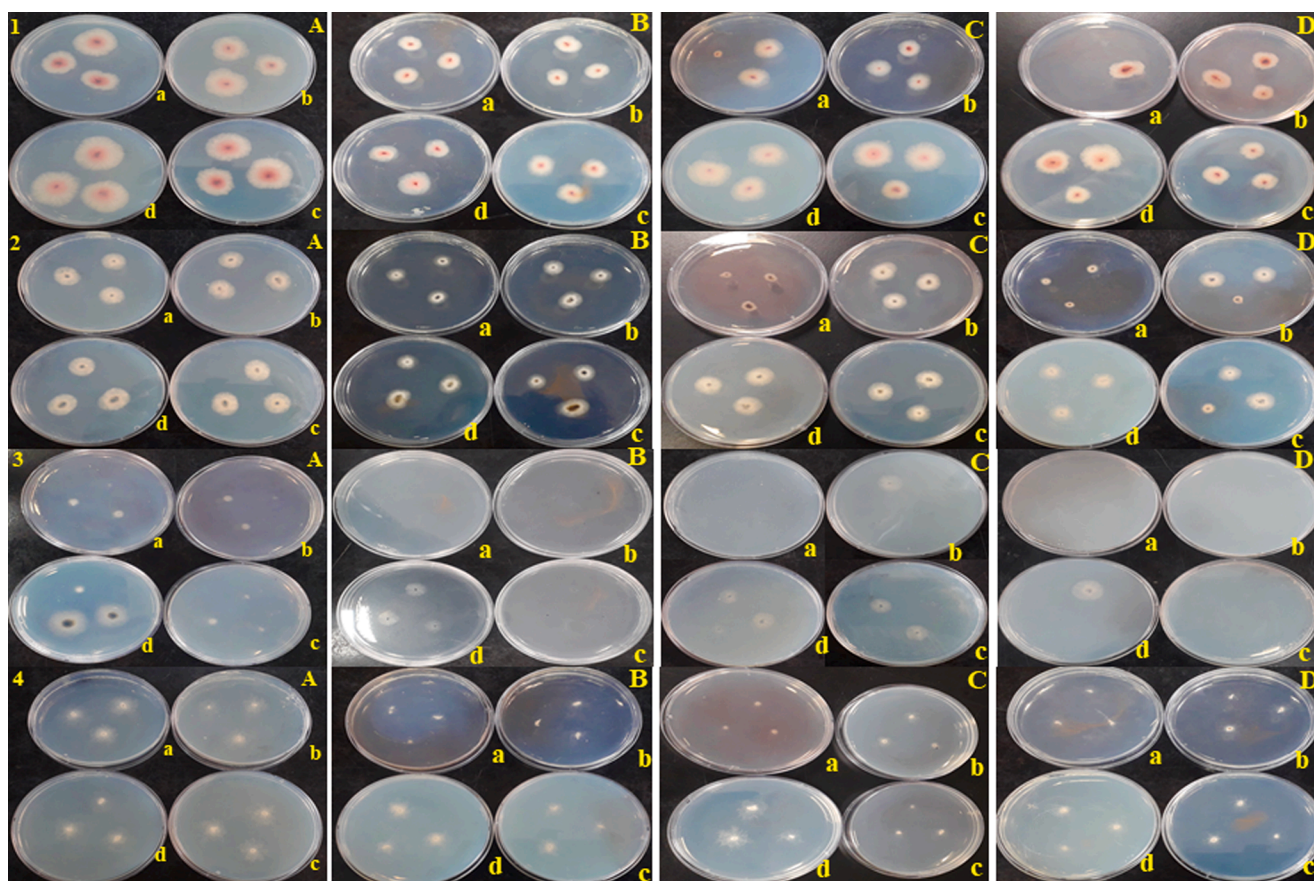
Fig. 9. Antifungal activity of (A) rGO (B) AuNPs (C) AgNPs (D) Ag/Au/rGO NC's through poison plate method. (1) *Fusarium graminearum* (2) *Alternaria alternata* (3) *Curvularia lunata* (4) *Sclerotinia sclerotiorum* (a) 2 mg (b) 1 mg (c) 500 μg (d) 50 μg concentration.

3.6. Nanomaterials against test fungal pathogens

The antifungal activity of the synthesized rGO, AgNPs, AuNPs, and Ag/Au/rGO NC's were performed using the poison plate method, and the results were presented in Table 4 & Fig. 9. The radial (vegetative) growth of foodborne fungal pathogens such as *Fusarium graminearum*, *Alternaria alternata* and phytopathogenic fungus of *Curvularia lunata* and *Sclerotinia sclerotiorum* were strongly inhibited by Ag/Au/rGO NC'S at the maximum test conc. of 2 mg/mL than other nanomaterials. Whereas the least inhibitory activity was observed for the lowest test conc. of 50 μg/mL and these results concluded the inhibitory actions were dose dependent. In addition, next to Ag/Au/rGO NC'S, AgNPs showed pronounced inhibitory activity in a dose dependent manner followed by AuNPs against all the test pathogens. Whereas, rGO alone did not show any inhibitory activity against the tested pathogens. The reason behind the enhanced antifungal activity of Ag/Au/rGO NC'S was due to pristine Ag and Au NPs in presence of several surface functional property of rGO leading to increased adsorption and affinity of fungal cell, resulting in higher exposure between fungal cell and Ag and Au NPs decorated on rGO platform. Our results are in agrees with the previous study (Sawangphruk, et al., 2012) in which the antifungal activity of reduced graphene oxide nanosheets against *Aspergillus niger*, *Aspergillus oryzae*, and *Fusarium oxysporum* was performed and concluded the fungitoxicity was in a concentration- dependent manner. A previous research work done by Cui et al. (2014) on graphene oxide loaded AgNPs act as antifungal materials, clearly concluded that the GO-Ag nanocomposites exhibit enhanced antifungal activity than pristine AgNPs. However, the level of significance of fungal inhibition of AgNPs and its nanocomposites varied between both types of fungi, as the highest inhibition activity was observed in phytopathogenic fungi when compared to foodborne fungi. This indicates that foodborne fungi are more susceptible, while phytopathogenic is more resistant. Furthermore, the level of significance also varied between AgNPs and nanocomposites agreeing with the study of Chen, et al., 2016, as they observed a 3–7-fold increase in the antifungal activity when they treated *Fusarium graminearum* with GO-AgNPs nanocomposite in comparison with AgNPs.

3.7. Invitro ZET test

The plant extract, rGO, AgNPs, AuNPs, and Ag/Au/rGO NC's of various concentrations were tested against zebrafish embryos (Fig. 10) in which all the test materials including plant leaves extract showed coagulation at higher concentrations (200 μg/mL). Whereas at 100 μg/mL, such a toxic effect was not observed in plant extract and the embryo was normal in architecture compared to control. But in the case of rGO delay in hatching was observed. Similarly, coagulation was observed for both AgNPs and Ag/Au/rGO NC's of up to 1.5 μg/mL concentration. But for AuNPs the coagulation was observed for up to 25 μg/mL concentration. At lower concentrations, both rGO and AuNPs displayed a normal embryo compared to control (0.09, 0.19, 0.39, 0.78, 1.56, 3.12, 6.25, 12.5) demonstrated the non-toxic effect. At 0.78 μg/mL concentration, tail bent and yolk sac edema was observed for AgNPs; Whereas Ag/Au/rGO NC's delay in hatching was observed. In continuous, the toxicity was observed for AgNPs at 0.19 μg/mL concentration; Whereas Ag/Au/rGO NC's at 0.39 μg/mL, the embryo hatched normally, indicating the reduced toxic effect. The reason for the reduced or diminished toxicity observed for Ag/Au/rGO NC's compared to AgNPs might be due to the possibility of pristine nanomaterials preservation in rGO matrix. There were no morphological changes observed for the control embryo throughout the experiments.
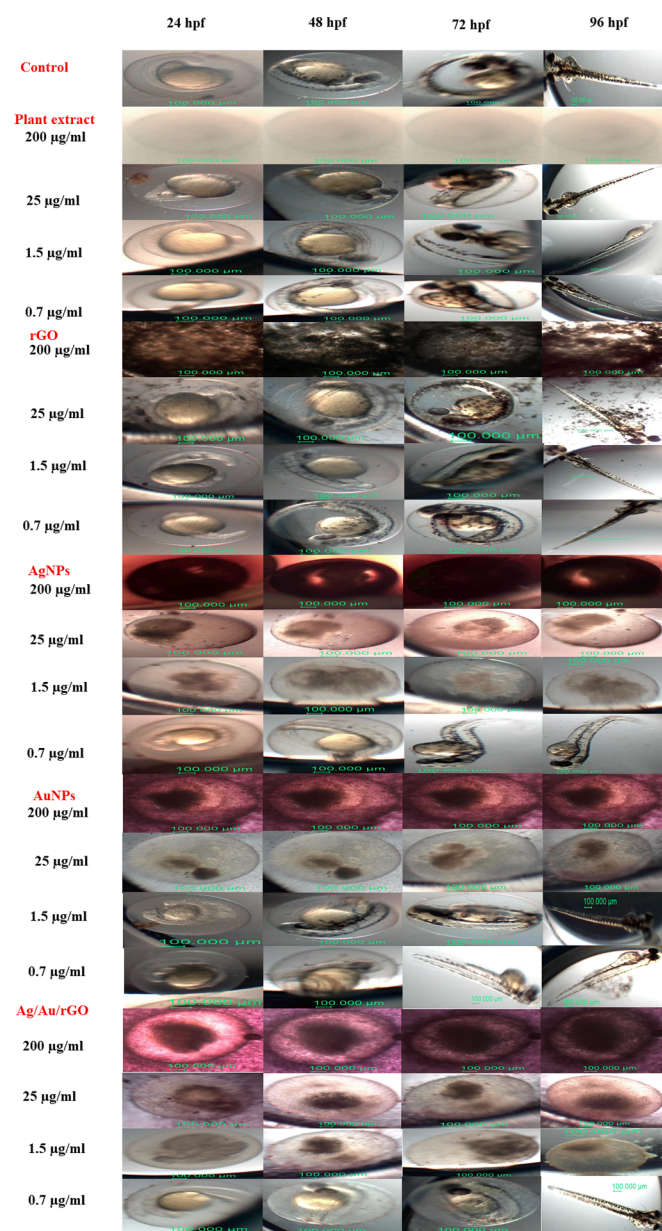
Fig. 10. Assessment of *in vitro* embryotoxicity of rGO, AgNPs, AuNPs, Ag/Au/rGO NC's. Control embryo followed by embryo interacted with leaves extract of *Allium cepa*, rGO, AgNPs, AuNPs, Ag/Au/rGO NC's at different time intervals (24, 48, 72 and 96 hpf).

4. Conclusions

By employing *Allium cepa Linn.* leaves extract, rGO, AgNPs, AuNPs, and Ag/Au/rGO NCs were successfully biofabricated. This was confirmed through various optical, spectral, and microscopic techniques. Using this method, rapid synthesis of AgNPs ranging from 1 to 30 nm and AuNPs ranging from 1 to 120 nm was achieved, and they were uniformly decorated on a thin silk-like appearance of a rGO sheet. Interestingly, the as-synthesized Ag/Au/rGO NC's modified electrode exhibited higher oxidation peak current (1.824 μA) and lower oxidation peak potential (0.92 V) value when compared to other modified glassy carbon electrodes such as bare GC (1.58 μA & 1.12 V), rGO (1.3 μA & 1.1 V), AgNPs (1.17 μA & 1.07 V), AuNPs (1.44 μA & 0.96 V) resulted in strong electrical conductivity and good electrocatalytic properties towards the electrooxidation of nitrite in neutral medium. Furthermore, Ag/Au/rGO NCs exhibited enhanced antibacterial efficiency against

Gram-negative bacteria and facilitated higher levels of ROS production compared to other nanomaterials. This, in turn, induced oxidative stress and ultimately led to bacterial death. Moreover, dose-dependent antifungal activity was observed against foodborne fungal pathogens, including *Fusarium graminearum*, *Alternaria alternata*, and phytopathogenic fungi like *Curvularia lunata* and *Sclerotinia sclerotiorum*, at the highest tested concentration of 2 mg/mL, surpassing the performance of other nanomaterials. The highest toxicity observed in zebrafish embryos was for AgNPs at 0.19 μg/mL, in contrast to Ag/Au/rGO NCs, which exhibited a toxicity level of 0.39 μg/mL. This indicates that Ag/Au/rGO NCs had a reduced toxic effect due to the presence of nanomaterials preserved within the rGO matrix. In conclusion, the synthesized Ag/Au/rGO NCs material appears to be suitable for development as both biomaterials in biomedical applications and effective sensors for environmental applications.

Role of the funding source

CRediT authorship contribution statement

Chandran Krishnaraj: Conceptualization, Methodology, Investigation, Formal analysis, Writing – original draft. **Sivaprakasam Radhakrishnan:** Methodology, Writing – review & editing. **Misgana Mengistu Asmare:** Writing – review & editing. **Shahid Wahab:** Writing – review & editing. **Byoung-Suhk Kim:** Writing – review & editing, Supervision. **Soon-Il Yun:** Writing – review & editing, Supervision, Project administration, Funding acquisition.

Declaration of competing interest

The authors declare that they have no known competing financial interests or personal relationships that could have appeared to influence the work reported in this paper.

Acknowledgements

Appendix A. Supplementary data

Supplementary data to this article can be found online at https://doi.org/10.1016/j.arabjc.2023.105379.

References

Alshorifi, F.T., Alswat, A.A., Salama, R.S., 2022. Gold-selenide quantum dots supported onto cesium ferrite nanocomposites for the efficient degradation of rhodamine B. Heliyon 8 (6), e09652.

Ardakani, T.S., Meidanchi, A., Shokri, A., Zadeh, A.S., 2020. Fe₃O₄@Au/reduced graphene oxide nanostructures: Combinatorial effects of radiotherapy and photothermal therapy on oral squamous carcinoma KB cell line. Ceram. Int. 46 (18), 28676–28685.

Ardakani, T.S., Meidanchi, A., Shokri, A., Zadeh, A.S., 2021. Structural and optical properties of Fe₃O₄@Au/rGO nanocomposites synthesized by hydrothermal method and their photothermal effect under NIR laser irradiation. Mater. Chem. Phys. 258, 123956.

Bahador, A., Pourakbari, B., Bolhari, B., Hashemi, F.B., 2015. In vitro evaluation of the antimicrobial activity of nanosilver-mineral trioxide aggregate against frequent anaerobic oral pathogens by a membrane-enclosed immersion test. Biomed. J. 38 (1), 77–83.

Baran, M.F., Keskin, C., Baran, A., Hatipoğlu, A., Yildiztekin, M., Küçükaydin, S., Kurt, K., Hoşgören, H., Sarker, M.M.R., Sufianov, A., Beylerli, O., Khalilov, R., Eftekhari, A., 2023. Green Synthesis of Silver Nanoparticles from *Allium cepa* L. Peel

Extract, Their Antioxidant, Antipathogenic, and Anticholinesterase Activity. Molecules 28 (5), 2310.

Boomi, P., Ganesan, R., Prabu Poorani, G., Jegatheeswaran, S., Balakumar, C., Gurumallesh Prabu, H., Anand, K., Marimuthu Prabhu, N., Jeyakanthan, J., Saravanan, M., 2020. Phyto-Engineered Gold Nanoparticles (AuNPs) with Potential Antibacterial, Antioxidant, and Wound Healing Activities Under in vitro and in vivo Conditions. Int. J. Nanomed. 15, 7553–7568.

Brennan, S.A., Ni Fhoghlu, C., Devitt, B.M., O'Mahony, F.J., Brabazon, D., Walsh, A., 2015. Silver nanoparticles and their orthopaedic applications. Bone. Joint. J. 97 (5), 582–589.

Buszewski, B., Railean-Plugaru, V., Pomastowski, P., Rafinska, K., Szultka-Mlynska, M., Golinska, P., Wypij, M., Laskowski, D., Dahm, H., 2018. Antimicrobial activity of biosilver nanoparticles produced by a novel *Streptacidiphilus durhamensis* strain. J. Microbiol. Immunol. Infect. 51 (1), 45–54.

Cai, Z., Yook, S., Lu, Y., Bergstrom, D., Winnik, M.A., Pignol, J.P., Reilly, R.M., 2017. Local Radiation Treatment of HER$_2$-Positive Breast Cancer Using Trastuzumab-Modified Gold Nanoparticles Labeled with ^{177}Lu. Pharm. Res. 34 (3), 579–590.

Cassar, S., Beekhuijzen, M., Beyer, B., Chapin, R., Dorau, M., Hoberman, A., Krupp, E., Leconte, I., Stedman, D., Stethem, C., Van den Oetelaar, D., Tornesi, B., 2019. A multi-institutional study benchmarking the zebrafish developmental assay for prediction of embryotoxic plasma concentrations from rat embryo-fetal development studies. Reprod. Toxicol. 86, 33–44.

Chen, J., Sun, L., Cheng, Y., Lu, Z., Shao, K., Li, T., Hu, C., Han, H., 2016. Graphene Oxide- Silver Nanocomposite: Novel Agricultural Antifungal Agent against *Fusarium graminearum* for Crop Disease Prevention. ACS Appl. Mater. Interfaces. 8 (36), 24057–24070.

Cui, J., Yang, Y., Zheng, M., Liu, Y., Xiao, Y., Lei, B., Chen, W., 2014. Facile fabrication of graphene oxide loaded with silver nanoparticles as antifungal materials. Mater. Res. Express. 1 (4), 045007.

De Mel, A., Chaloupka, K., Malam, Y., Darbyshire, A., Cousins, B., Seifalian, A.M., 2012. A silver nanocomposite biomaterial for blood-contacting implants. J. Biomed. Mater. Res. A. 100 (9), 2348–2357.

El-Deeb, N.M., Khattab, S.M., Abu-Youssef, M.A., Badr, A.M.A., 2022. Green synthesis of novel stable biogenic gold nanoparticles for breast cancer therapeutics via the induction of extrinsic and intrinsic pathways. Sci. Rep. 12 (1), 11518.

El-Maghrabi, N., El-Borady, O.M., Hosny, M., Fawzy, M., 2021. Catalytic and Medical Potential of a Phyto-Functionalized Reduced Graphene Oxide-Gold Nanocomposite Using Willow- Leaved Knotgrass. ACS Omega. 6 (50), 34954–34966.

Franci, G., Falanga, A., Galdiero, S., Palomba, L., Rai, M., Morelli, G., Galdiero, M., 2015. Silver Nanoparticles as Potential Antibacterial Agents. Molecules. 20 (5), 8856–8874.

Ge, L., Li, Q., Wang, M., Ouyang, J., Li, X., Xing, M.M., 2014. Nanosilver particles in medical applications: synthesis, performance, and toxicity. Int. J. Nanomed. 9, 2399–2407.

Geim, A.K., Novoselov, K.S., 2007. The rise of graphene. Nat. Mater. 6 (3), 183–191.

Gurunathan, S., 2015. Biologically synthesized silver nanoparticles enhance antibiotic activity against Gram-negative bacteria. J. Ind. Eng. Chem. 29, 217–226.

Gurunathan, S., Han, J.W., Kwon, D.N., Kim, J.H., 2014. Enhanced antibacterial and anti- biofilm activities of silver nanoparticles against Gram-negative and Gram-positive bacteria. Nanoscale Res. Lett. 9 (1), 373.

Han, L., Cui, S., Deng, D., Li, Y., Yan, X., He, H., Luo, L., 2020. Synthesis of Ag-Au/Reduced Graphene Oxide/TiO$_2$ Nanocomposites: Application as a Non- enzymatic Amperometric H$_2$O$_2$ Sensor. Curr. Anal. Chem. 16 (4), 485–492.

Hazarika, M., Sonowal, S., Saikia, I., Boruah, P.K., Das, M.R., Tamuly, C., 2017. Biogenic synthesis of Ag–Au–In decorated on rGO nanosheet and its antioxidant and biological activities. Mater. Res. Express. 4, 095013.

Ibrahim, A.A., Salama, R.S., El-Hakam, S.A., Khder, A.S., Ahmed, A.I., 2021. Synthesis of sulfated zirconium supported MCM-41 composite with high-rate adsorption of methylene blue and excellent heterogeneous catalyst. Colloids Surf. A Physicochem. Eng. 616, 126361.

Ipek, P., Baran, M.F., Baran, A., Hatipoğlu, A., Keskin, C., Yildiztekin, M., Küçükaydin, S., Becerekli, H., Kurt, K., Eftekhari, A., Huseynova, I., Khalilov, R., Cho, W.C., 2023. Green synthesis and evaluation of antipathogenic, antioxidant, and anticholinesterase activities of gold nanoparticles (Au NPs) from *Allium cepa* L. peel aqueous extract. Biomass Conv. Bioref. https://doi.org/10.1007/s13399-023-04362-y.

Iravani, S., Korbekandi, H., Mirmohammadi, S.V., Zolfaghari, B., 2014. Synthesis of silver nanoparticles: chemical, physical and biological methods. Res Pharm Sci. 9 (6), 385–406.

Jain, J., Arora, S., Rajwade, J.M., Omray, P., Khandelwal, S., Paknikar, K.M., 2009. Silver Nnoparticles in Therapeutics: Development of an Antimicrobial Gel Formulation for Topical Use. Mol. Pharm. 6 (5), 1388–1401.

Joshi, A.S., Singh, P., Mijakovic, I., 2020. Interactions of Gold and Silver Nanoparticles with Bacterial Biofilms: Molecular Interactions behind Inhibition and Resistance. Int. J. Mol. Sci. 21 (20), 7658.

Khanam, P.N., Hasan, A., 2019. Biosynthesis and characterization of graphene by using non-toxic reducing agent from *Allium Cepa* extract: Anti-bacterial properties. Int. J. Biol. Macromol. 126, 151–158.

Khatua, A., Priyadarshini, E., Rajamani, P., Patel, A., Kumar, J., Naik, A., Saravanan, M., Barabadi, H., Prasad, A., Ghosh, I., Paul, B., Meena, R., 2020. Phytosynthesis, Characterization and Fungicidal Potential of Emerging Gold Nanoparticles Using *Pongamia pinnata* Leave Extract: A Novel Approach in Nanoparticle Synthesis. J. Clust. Sci. 31 (1), 125–131.

Krishnaraj, C., Jagan, E.G., Rajasekar, S., Selvakumar, P., Kalaichelvan, P.T., Mohan, N., 2010. Synthesis of silver nanoparticles using *Acalypha indica* leaf extracts and its

antibacterial activity against water borne pathogens. Colloids Surf. B Biointerfaces 76 (1), 50–56.

Krishnaraj, C., Harper, S.L., Choe, H.S., Kim, K.P., Yun, S.I., 2015. Mechanistic aspects of biologically synthesized silver nanoparticles against food- and water-borne microbes. Bioprocess Biosyst. Eng. 38 (10), 1943–1958.

Krishnaraj, C., Kaliannagounder, V.K., Rajan, R., Ramesh, T., Kim, C.S., Park, C.H., Liu, S., Yun, S.I., 2022a. Silver nanoparticles decorated reduced graphene oxide: Eco-friendly synthesis, characterization, biological activities and embryo toxicity studies. Environ. Res. 210, 112864.

Krishnaraj, C., Radhakrishnan, S., Ramachandran, R., Ramesh, T., Kim, B.S., Yun, S.I., 2022b. In vitro toxicological assessment and biosensing potential of bioinspired chitosan nanoparticles, selenium nanoparticles, chitosan/selenium nanocomposites, silver nanoparticles and chitosan/silver nanocomposites. Chemosphere 301, 134790.

Kumar, S., Ojha, A.K., Walkenfort, B., 2016. Cadmium oxide nanoparticles grown in situ on reduced graphene oxide for enhanced photocatalytic degradation of methylene blue dye under ultraviolet irradiation. J. Photochem. Photobiol. B. 159, 111–119.

Lackner, P., Beer, R., Broessner, G., Helbok, R., Galiano, K., Pleifer, C., Pfausler, B., Brenneis, C., Huck, C., Engelhardt, K., Obwegeser, A.A., Schmutzhard, E., 2008. Efficacy of silver nanoparticles-impregnated external ventricular drain catheters in patients with acute occlusive hydrocephalus. Neurocrit. Care. 8 (3), 360–365.

Lammer, E., Carr, G.J., Wendler, K., Rawlings, J.M., Belanger, S.E., Braunbeck, T., 2009. Is the fish embryo toxicity test (FET) with the zebrafish (*Danio rerio*) a potential alternative for the fish acute toxicity test? Comp. Biochem. Physiol. C Toxicol. Pharmacol. 149 (2), 196–209..

Lee, W., Kim, K.J., Lee, D.G., 2014. A novel mechanism for the antibacterial effect of silver nanoparticles on *Escherichia coli*. Biometals. 27 (6), 1191–1201.

Lekshmi, P., Sumi, S.B., Viveka, S., Jeeva, S., Raja Brindha, J., 2012. Antibacterial activity of nanoparticles from *Allium* sp. J. Microbiol. Biotechnol. Res. 2 (1), 115–119.

Li, J., Liu, C., 2010. Ag/Graphene Heterostructures: Synthesis, Characterization and Optical Properties. Eur. J. Inorg. Chem. 1244–1248.

Liu, C., Liu, H., Zhang, K., Dou, M., Pan, B., He, X., Lu, C., 2019. Partly reduced graphene oxide aerogels induced by proanthocyanidins for efficient dye removal. Bioresour. Technol. 282, 148–155.

Lu, C.H., Yang, H.H., Zhu, C.L., Chen, X., Chen, G.N., 2009. A graphene platform for sensing biomolecules. Angew. Chem. Int. Ed. 48 (26), 4785–4787.

Maddinedi, S.B., Mandal, B.K., Vankayala, R., Kalluru, P., Pamanji, S.R., 2015. Bioinspired reduced graphene oxide nanosheets using *Terminalia chebula* seeds extract. Spectrochim. Acta A Mol. Biomol. Spectrosc. 145, 117–124.

Mannaa, M.A., Qasim, K.F., Alshorifi, F.T., El-Bahy, S.M., Salama, R.S., 2021. Role of NiO Nanoparticles in Enhancing Structure Properties of TiO$_2$ and Its Applications in Photodegradation and Hydrogen Evolution. ACS Omega. 6 (45), 30386–30400.

Meidanchi, A., 2020. Cobalt ferrite nanoparticles supported on reduced graphene oxide sheets: optical, magnetic and magneto-antibacterial studies. Nanotechnology. 31 (44), 445704.

Mnayer, D., Fabiano-Tixier, A.S., Petitcolas, E., Hamieh, T., Nehme, N., Ferrant, C., Fernandez, X., Chemat, F., 2014. Chemical composition, antibacterial and antioxidant activities of six essentials oils from the *Alliaceae* family. Molecules. 19 (12), 20034–20053.

Moghayedi, M., Goharshadi, E.K., Ghazvini, K., Ahmadzadeh, H., Ranjbaran, L., Masoudi, R., Ludwig, R., 2017. Kinetics and mechanism of antibacterial activity and cytotoxicity of Ag-RGO nanocomposite. Colloids Surf. B Biointerfaces 159, 366–374.

Moon, I.K., Lee, J., Ruoff, R.S., Lee, H., 2010. Reduced graphene oxide by chemical graphitization. Nat. Commun. 1 (1), 73.

Muddassir, M., Raza, A., Munir, S., Basirat, A., Ahmed, M., Butt, M.S., Dar, O.A., Ahmed, S., Shamim, S., Naqvi, S.Z.H., 2022. Antibacterial efficacy of silver nanoparticles (AgNPs) against metallo-β-lactamase and extended spectrum β-lactamase producing clinically procured isolates of *Pseudomonas aeruginosa*. Sci. Rep. 12 (1), 20685.

Murphy, M., Ting, K., Zhang, X., Soo, C., Zheng, Z., 2015. Current Development of Silver Nanoparticle Preparation, Investigation, and Application in the Field of Medicine. J. Nanomater. 696918.

Nasraoui, S., Al-Hamry, A., Teixeira, P.R., Ameur, S., Paterno, L.G., Ben Ali, M., Kanoun, O., 2021. Electrochemical sensor for nitrite detection in water samples using flexible laser- induced graphene electrodes functionalized by CNT decorated by Au nanoparticles. J. Electroanal. Chem. 880, 114893.

Parida, U.K., Bindhani, B.K., Nayak, P., 2011. Green Synthesis and Characterization of Gold Nanoparticles Using Onion (Allium cepa) Extract. World J. Nano Sci. Eng. 1, 93–98.

Patra, J.K., Baek, K.H., 2016. Biosynthesis of silver nanoparticles using aqueous extract of silky hairs of corn and investigation of its antibacterial and anticandidal synergistic activity and antioxidant potential. IET Nanobiotechnol. 10 (5), 326–333.

Radhakrishnan, S., Krishnamoorthy, K., Sekar, C., Wilson, J., Kim, S.J., 2014. A highly sensitive electrochemical sensor for nitrite detection based on Fe$_2$O$_3$ nanoparticles decorated reduced graphene oxide nanosheets. Appl. Catal. B: Environ. 148-149, 22–28.

Rajan, R., Chandran, K., Harper, S.L., Yun, S.I., Kalaichelvan, P.T., 2015. Plant extract synthesized silver nanoparticles: An ongoing source of novel biocompatible materials. Ind. Crop Prod. 70, 356–373.

Rigo, C., Ferroni, L., Tocco, I., Roman, M., Munivrana, I., Gardin, C., Cairns, W.R., Vindigni, V., Azzena, B., Barbante, C., Zavan, B., 2013. Active Silver Nanoparticles for Wound Healing. Int. J. Mol. Sci. 14 (3), 4817–4840.

Sawangphruk, M., Srimuk, P., Chiochan, P., Sangsri, T., Siwayaprahm, P., 2012. Synthesis and antifungal activity of reduced graphene oxide nanosheets. Carbon. 50 (14), 5156–5161.

Shah, M.Z., Guan, Z.H., Din, A.U., Ali, A., Rehman, A.U., Jan, K., Faisal, S., Saud, S., Adnan, M., Wahid, F., Alamri, S., Siddiqui, M.H., Ali, S., Nasim, W., Hammad, H.M., Fahad, S., 2021. Synthesis of silver nanoparticles using *Plantago lanceolata* extract and assessing their antibacterial and antioxidant activities. Sci. Rep. 11 (1), 20754.

Singh, P., Mijakovic, I., 2022. Green synthesis and antibacterial applications of gold and silver nanoparticles from *Ligustrum vulgare* berries. Sci. Rep. 12 (1), 7902.

Stine, R., Robinson, J.T., Sheehan, P.E., Tamanaha, C.R., 2010. Real-time DNA detection using reduced graphene oxide field effect transistors. Adv. Mater. 22 (46), 5297–5300.

Tian, Y., Yu, Z., Cao, L., Zhang, X.L., Sun, C., Wang, D.W., 2021. Graphene oxide: An emerging electro material for energy storage and conversion. J. Energy Chem 55, 323–344.

Tiwari, D.K., Behari, J., Sen, P., 2008. Time and dose-dependent antimicrobial potential of Ag nanoparticles synthesized by top-down approach. Curr. Sci. 95 (5), 647–655.

Urnukhsaikhan, E., Bold, B.E., Gunbileg, A., Sukhbaatar, N., Mishig-Ochir, T., 2021. Antibacterial activity and characteristics of silver nanoparticles biosynthesized from *Carduus crispus*. Sci. Rep. 11 (1), 21047.

Velázquez-Velázquez, J.L., Santos-Flores, A., Araujo-Meléndez, J., Sánchez-Sánchez, R., Velasquillo, C., González, C., Martínez -Castañon, G., Martinez-Gutierrez, F., 2015. Anti-biofilm and cytotoxicity activity of impregnated dressings with silver nanoparticles. Mater. Sci. Eng. C. 49, 604–611.

Vellaichamy, B., Periakaruppan, P., 2016. A facile, one-pot and eco-friendly synthesis of gold/silver nanobimetallics smartened rGO for enhanced catalytic reduction of hexavalent chromium. RSC Adv. 6, 57380–57388.

Willcox, M.D.P., Hume, E.B.H, Vijay, A.K., Petcavich, R., 2010. Ability of silver-impregnated contact lenses to control microbial growth and colonisation. J 3, 143–148.

Wu, J., Lin, H., Moss, D.J., Loh, K.P., Jia, B., 2023. Graphene oxide for photonics, electronics and optoelectronics. Nat. Rev. Chem. 7, 162–183.

Xuan, Y., Wu, Y.Q., Shen, T., Qi, M., Capano, M.A., Cooper, J.A., Ye, P.D., 2008. Atomic-layer-deposited nanostructures for graphene-based nanoelectronics. Appl. Phys. Lett. 92 (1), 013101.

Yamanaka, M., Hara, K., Kudo, J., 2005. Bactericidal actions of a silver ion solution on *Escherichia coli*, studied by energy-filtering transmission electron microscopy and proteomic analysis. Appl. Environ. Microbiol. 71 (11), 7589–7593.

Yaragalla, S., Rajendran, R., Jose, J., AlMaadeed, M.A., Kalarikkal, N., Thomas, S., 2016. Preparation and characterization of green graphene using grape seed extract for bioapplications. Mater Sci Eng C. Mater Biol Appl. 65, 345–353.

Zhang, Y.L., Li, J.C., Zhou, H., Liu, Y.Q., Han, D.D., Sun, H.B., 2021b. Electro-responsive actuators based on graphene. The Innovation 2 (4), 100168.

Zhang, S., Lu, Q., Zhang, C., Zhou, Y., Liu, M., Zhang, Y., Deng, L., 2022. Green Synthesis of Silver-Carbon Nanocomposites with Extraordinary Stability and Robust Antibacterial Activity against Bacterial Diseases in Fish. ACS Appl. Bio. Mater. 5 (3), 1064–1072.

Zhang, Y., Mahdavi, B., Mohammadhosseini, M., Rezaei-Seresht, E., Paydarfard, S., Qorbani, M., Karimian, M., Abbasi, N., Ghaneialvar, H., Karimi, E., 2021a. Green synthesis of NiO nanoparticles using *Calendula officinalis* extract: Chemical charactrization, antioxidant, cytotoxicity, and anti-esophageal carcinoma properties. Arab. J. Chem. 14 (5), 103105.

Zheng, Q., Li, Z., Yang, J., Kim, J.K., 2014. Graphene oxide-based transparent conductive films. Prog. Mater Sci. 64, 200–247.